Article

Institution of MECHANICAL ENGINEERS
Journal of MECHANICAL ENGINEERING SCIENCE

Proc IMechE Part C:
J Mechanical Engineering Science
2018, Vol. 232(7) 1247–1254

DOI: 10.1177/0954406216683974
journals.sagepub.com/home/pic
SAGE

Resonant frequencies of perforated plates with rectangular slots

Oumar R Barry and Emadeddin Y Tanbour

Abstract

Most previous work on perforated plates employed elasticity theory to determine equivalent material properties that make the deflection of the solid plate identical to that of the perforated plate. However, it will be inaccurate to utilize the proposed elastic properties to predict the natural frequencies of a perforated plate. In this paper, the free vibrations of perforated plates with rectangular slots and rectangular slot-patterns are examined using theoretical and finite-element methods. The natural frequencies are obtained for various cases of perforations. An explicit expression is obtained for the equivalent elastic properties using the regression analysis method. These effective material properties are used in a solid-plate model to predict the natural frequencies of the corresponding perforated plate. To validate the theoretical analysis, the effective resonant frequencies are compared with the exact natural frequencies of the perforated plates. Parametric studies are conducted to examine the effect of both parallel and perpendicular ligament efficiencies on the resonant frequencies.

Keywords

Free vibration, flame arrestor, natural frequency, perforated plate, rectangular perforation, mode shape, analytical methods

Date received: 25 April 2016; revised: 23 September 2016; accepted: 14 November 2016

Introduction

In the last few decades, perforated plates have received considerable attention because of their widespread applications in acoustic performance, heat exchanger, heat dissipation, weight reduction, and many other engineering applications. In the design of a heat exchanger, perforated plates are employed to achieve high heat transfer efficiency by controlling tube spacing and allowing the baffle effect on the flow. Perforated plates with rectangular slots are installed in the main combustion air inlet of many domestic and commercial appliances with standing or powered ignition sources to prevent flame flashback.

The study of perforated plates abounds in the literature. However, most investigations are limited to static stress–strain problems. O'Donnell and Langer[1] are among the first authors to study perforated plates using generalized plane strain and stress theory. They present a method for calculating stresses and deformations in perforated plates with circular slots and triangular slot-patterns. Further work by Slot and O'Donnell[2] provided effective elastic constants for thick plates with circular perforations having both square and triangular slot-patterns. The effective elastic constants of a thin perforated plate with circular slots were examined.[3–5] It was found that these elastic constants are significantly dependent on the ligament efficiency. The proposed methods for determining the effective elastic constants in the aforementioned papers have limited applications, in that they are only valid for static analysis. Jhung and Yu[6] showed that the classical method for determining equivalent elastic properties cannot be used to accurately predict the natural frequencies of perforated plate. To close this gap, numerous authors used other methods, such as finite-element methods, to examine the natural frequencies of perforated plates.[6–9] Burgemeister and Hansen[7] presented a free-vibration analysis of a simply supported perforated plate with circular holes and rectangular slot-patterns. Their findings agree with those of Jhung and Yu.[6]

Many attempts have been made to understand the free vibration of perforated plates. However, most of these studies are limited to circular perforations with

School of Engineering and Technology, Central Michigan University, USA

Corresponding author:
Oumar R Barry, Central Michigan University Mt. Pleasant, MI 48859, USA.
Email: barry1o@cmich.edu

triangular or square slot-patterns. To our knowledge, there have been no attempts to study rectangular perforations with rectangular slot-patterns, which are useful in industrial applications. In combustion applications where perforated flame arrestors are used to prevent flame flashout, rectangular perforations are preferred over other shapes, owing to the need to increase air flow to satisfy combustion. Rectangular perforations allow designers of flame arrestors to increase air flow while keeping the shorter side of the rectangular perforation small enough to lift the flame and keep it anchored inside the combustion system. It has been observed in the appliance industry that the air flow through perforated flame arrestors opposed by flame propagation inside a combustion system is a major cause of combustion-induced vibrations. This paper examines the free vibration of perforated plates with rectangular slots and rectangular slot-patterns using both theoretical and finite-element methods. Regression analysis is conducted to determine the equivalent elastic properties of the perforated plates. These equivalent elastic properties are then used in the theoretical analysis to predict the effective natural frequencies (i.e., natural frequencies of the equivalent plate). The validity of the theoretical analysis is examined by comparing the exact natural frequency of the perforated plate modeled in SolidWorks® with that of the equivalent plate. Parametric studies are conducted to examine the effect of parallel and perpendicular ligament efficiencies on the natural frequencies.

Description of the system

The system of interest is depicted in Figure 1. The rectangular plate is assumed to be clamped at all edges and has the following geometry parameters: length a, width b, thickness h. The perforation geometry is rectangular, with width d and height c. The ligament efficiencies in the parallel and perpendicular directions are given in equations (1) and (2), respectively. Each ligament efficiency depends on the size of the slot (c or d) and the distance separating the slots (P_x or P_y)

$$\eta_x = 1 - \frac{d}{P_x} \tag{1}$$

$$\eta_y = 1 - \frac{c}{P_y} \tag{2}$$

The density of the perforated plate is expressed as

$$\rho^* = \rho\left(1 - \frac{cd}{P_x P_y}\right) \tag{3}$$

where ρ denotes the density of the solid plate.

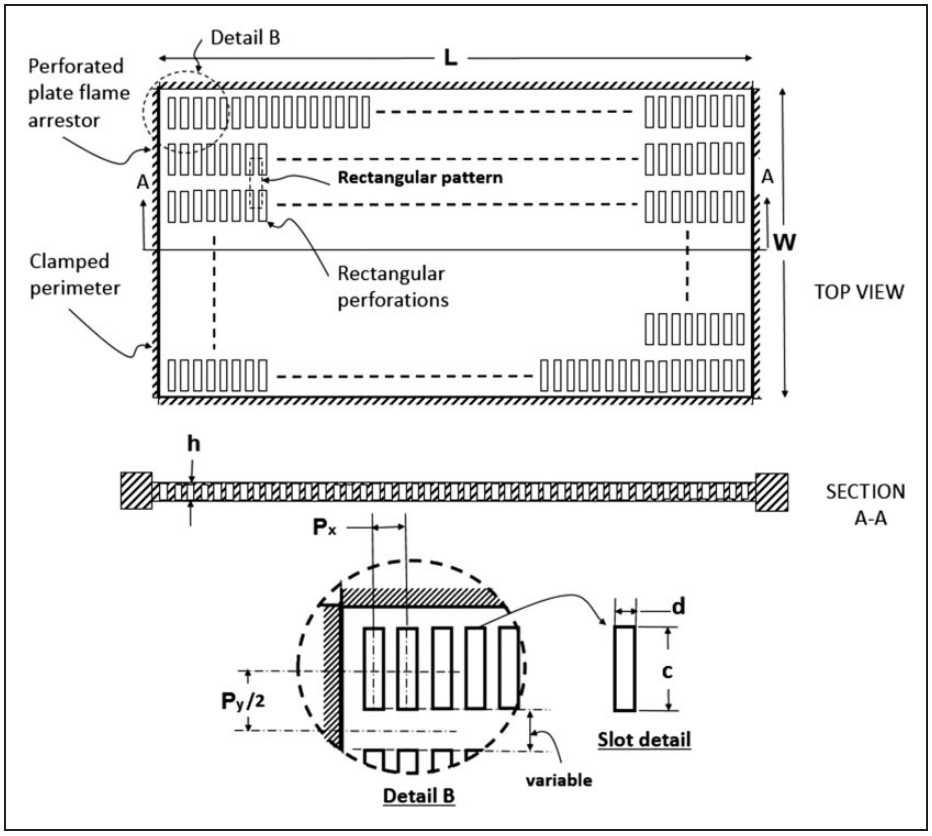

Figure 1. Arrangement of perforated plate flame arrestor.

The governing equation of motion for the free vibration of an isotropic thin plate is given as[10–17]

$$D\nabla^4 w(x,y,t) + \rho h \frac{\partial^2 w}{\partial t^2}(x,y,t) = 0 \tag{4}$$

where

$$\nabla^4 = \frac{\partial^4}{\partial x^4} + 2\frac{\partial^4}{\partial x^2 \partial y^2} + \frac{\partial^4}{\partial y^4} \tag{5}$$

and

$$D = \frac{Eh^3}{12(1-\nu^2)} \tag{6}$$

where D is the flexural rigidity of the plate, $w(x,y,t)$ is the transverse displacement, ρ is the density of the plate, h is the thickness of the plate, E is the modulus of elasticity, and ν is the Poisson ratio. Note that the solid plate is isotropic and homogeneous; as such, ρ is constant throughout. The density of the perforated plate is dependent on the solid area fraction of the panel and the density of the solid plate, as shown in equation (3).

Following Bhat,[18] the nondimensional frequency can be expressed as

$$\lambda = \frac{\rho h \omega^2 a^4}{D} \tag{7}$$

where ω denotes the circular natural frequency.

From equation (7), the natural frequency of a plate is proportional to the square root of the flexural rigidity. The ratio of the flexural rigidity of the perforated plate to that of the solid plate is then equal to the square of the natural frequency ratio. Therefore, the ratio of the flexural rigidity can be approximated to be the same as the ratio of modulus of elasticity (E^*/E) because the small change in the Poisson ratio can be negligible in the calculation of the resonant frequencies. Hence, the ratio of the modulus of elasticity can be expressed as

$$\frac{E^*}{E} = \frac{\rho^*}{\rho}\left(\frac{\omega^*}{\omega}\right)^2 \tag{8}$$

The finite-element analysis was conducted using the equation

$$(\mathbf{K} - \omega^2 \mathbf{M})\mathbf{U} = \mathbf{0} \tag{9}$$

Where $\mathbf{U}$ is the vector of nodal displacement and $\mathbf{K}$ and $\mathbf{M}$, respectively, denote the stiffness and mass matrix. For nontrivial solutions, equation (9) becomes $\mathbf{K} = \omega^2 \mathbf{M}$. This represents the generalized eigenvalues problem, which is used to determine the natural frequencies.

Numerical simulation

The variables for the 10 cases of perforation size studied are given in Table 1. The material properties of the stainless steel used for the numerical analysis are listed in Table 2. All finite-element analysis is

Table 1. Variable perforation sizes for $a = 100$ mm, $b = 100$ mm, $h = 0.5$ mm, $d = 1.5$ mm.

Case	c	P_x	P_y
1	3	2.5	4.0
2	3	3.0	5.0
3	3	3.5	5.5
4	3	4.0	6.0
5	3	4.5	6.5
6	3	5.0	7.0
7	3	5.5	7.5
8	3	6.0	8.0
9	3	6.5	8.5
10	3	7.0	9.0

Table 2. Mechanical properties of 316 stainless steel sheet (AK Steel).

Property	Value	Units
Elastic modulus	193	GPa
Poisson ratio	0.27	–
Mass density	8000	kg/m^3
Tensile strength	580.0	MPa
Yield strength	172.37	MPa

Table 3. Validation of frequency parameters $\sqrt{\lambda}$.

Side ratio (α)	Mode	Th. value	FEA value	% Error
1	1	35.9855	36.1080	0.3141
	2	73.3950	73.6801	0.4794
	3	73.3950	73.6855	0.1739
	4	108.2200	108.9052	0.2564
	5	131.7800	132.1284	0.1753
1.5	1	60.8176	60.7521	0.1079
	2	93.9156	93.8235	0.0982
	3	148.8996	148.7758	0.0832
	4	149.7980	149.8822	0.0562
	5	179.7057	179.5562	0.0832
2	1	98.5914	98.9011	0.3392
	2	128.0580	128.6719	0.3869
	3	181.2000	181.5151	0.3942
	4	256.3822	257.0395	0.6292
	5	257.1591	257.6100	0.2637

FEA: finite-element analysis; Th.: theoretical.

conducted utilizing SolidWorks® Simulations. Each numerical simulation accounts for high-quality meshing with four-point Jacobian points and a maximum element size of 1 mm, resulting in approximately 300,000 nodes for each case. The selected solver is based on the preconditioned conjugate gradient iterative method. The first numerical analysis is to check the accuracy of the finite-element analysis simulation. Three solid plates, each with a different aspect ratio ($\alpha = 1$, 1.5, and 2), are examined and the

Table 4. Resonant frequencies for the first 20 modes of 10 cases.

	Frequency (rad/s)									
Mode	Case 1	Case 2	Case 3	Case 4	Case 5	Case 6	Case 7	Case 8	Case 9	Case 10
1	1684.9	1814.3	1849.0	1815.8	1869.5	1927.0	1903.5	1886.2	1933.0	1926.7
2	2466.9	2684.5	2720.6	2742.5	2809.2	2896.3	2880.3	2876.7	2924.3	2939.9
3	3789.3	4158.2	4203.6	4307.8	4401.2	4540.3	4534.9	4551.9	4606.3	4653.7
4	4210.5	4510.1	4601.5	4487.2	4629.1	4754.5	4702.9	4642.7	4769.0	4744.4
5	4970.4	5343.2	5433.5	5366.6	5518.9	5666.6	5622.3	5573.5	5699.2	5694.3
6	5621.6	6200.6	6264.0	6473.1	6606.4	6817.6	6825.9	6869.8	6937.4	7024.6
7	6242.8	6747.3	6840.9	6853.3	7026.5	7216.0	7184.0	7155.3	7283.0	7309.5
8	7943.5	8563.7	8734.3	8522.3	8795.6	9004.0	8928.9	8809.2	9046.2	9007.6
9	8013.1	8719.7	8824.9	8944.4	9151.6	9403.2	9389.3	9387.9	9522.4	9590.1
10	8022.6	8789.2	8878.4	9215.1	9400.2	9701.5	9728.7	9722.8	9892.2	9937.6
11	8768.2	9388.0	9557.2	9389.5	9671.9	9898.7	9831.8	9805.6	9957.6	10027.0
12	10028.0	10768.0	10938.0	10846.0	11146.0	11407.0	11354.0	11265.0	11498.0	11508.0
13	10300.0	11249.0	11375.0	11627.0	11882.0	12215.0	12224.0	12258.0	12405.0	12522.0
14	10746.0	11911.0	12033.0	12521.0	12770.0	13178.0	13231.0	13346.0	13458.0	13645.0
15	11787.0	12705.0	12882.0	12896.0	13224.0	13539.0	13506.0	13446.0	13678.0	13732.0
16	13065.0	13957.0	14224.0	13909.0	14355.0	14647.0	14572.0	14370.0	14742.0	14701.0
17	13082.0	14323.0	14480.0	14771.0	15195.0	15533.0	15468.0	15279.0	15646.0	15624.0
18	13839.0	14779.0	15045.0	14892.0	15236.0	15640.0	15677.0	15752.0	15918.0	16091.0
19	14015.0	15193.0	15386.0	15534.0	15902.0	16290.0	16283.0	16258.0	16497.0	16597.0
20	14048.0	15560.0	15726.0	16220.0	16688.0	17028.0	16975.0	16806.0	17168.0	17175.0

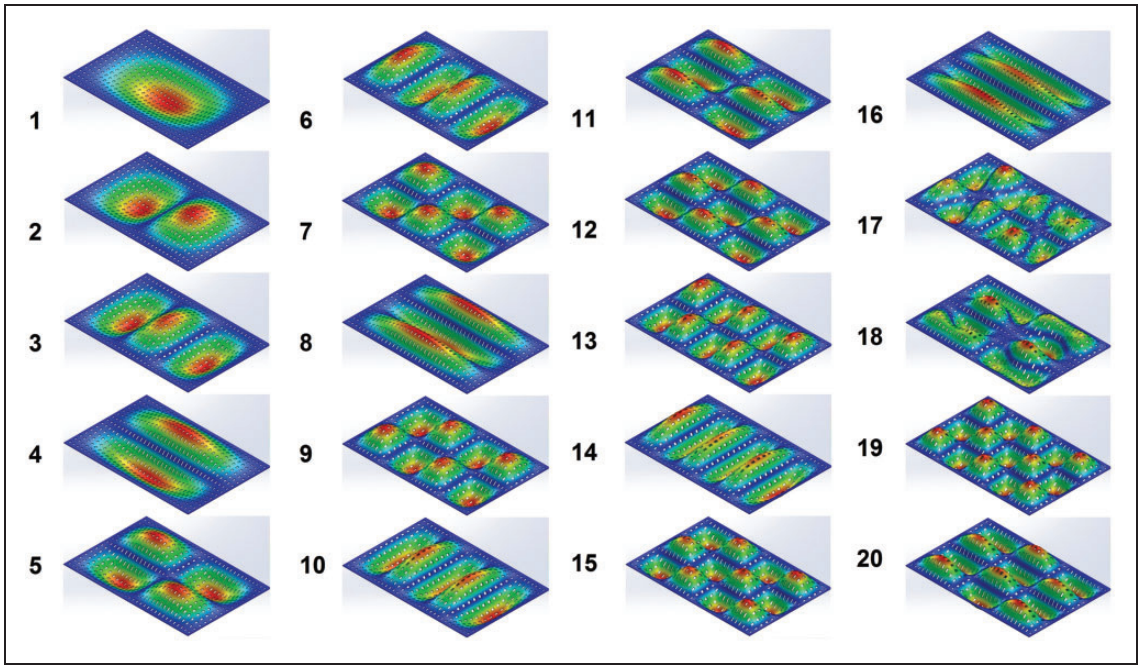

Figure 2. Mode shapes for Case 5.

dimensionless natural frequencies are obtained using two methods. The first method is that of Bhat[18] using Matlab® and the second is from the finite-element analysis in SolidWorks®. The results are listed in Table 3 and show very good agreement, with a maximum percentage of error of 0.63%. The theoretical results in Table 3 are also in good agreement with those of Bhat.[18] This reinforces the accuracy of the theoretical results and is an indication that the utilized mesh refinement in SolidWorks® is adequate to model the free vibration of the rectangular plates.

It should be noted that the remaining numerical examples are solely based on $\alpha = 1.5$. Free-vibration analyses of perforated plates are conducted for the 10 cases listed in Table 1. The resonant frequencies for each case are listed in Table 4 and the mode shapes for Case 5 are depicted in Figure 2. The results from Table 4 indicate that the resonant frequencies of all the perforated cases are smaller than those of the solid plate; the case with the most perforations (case 1) yields the smallest resonant frequencies. This is expected, as the case with the most open area has the smallest density.

The next step is to determine the effective elastic constant for the perforation cases using regression analysis in combination with the natural frequencies of the perforated cases obtained in SolidWorks®. Since the ratio of the natural frequency is independent of the mode number, the overall natural frequency ratio (ω^*/ω) is obtained by taking the average of the individual natural frequency ratios over all the modes. This is done for all the 10 perforated cases, where each case correspondents to one frequency ratio. A plot of this ratio against the ligament efficiency in the x and y directions is shown in Figure 3. The results in this figure indicate that the ligament efficiency in both directions increases with the natural frequency ratio.

Regression analysis is then conducted in Matlab® using the data from Figure 3 to determine the curve of best fit. This curve is presented in equation (10) and is dependent on both ligament efficiency (η_x and η_y)

$$\frac{E^*}{E} = \frac{\rho^*}{\rho}\left(P_0 + P_{10}\eta_x + P_{01}\eta_y + P_{11}\eta_x\eta_y + P_{20}\eta_x^2 + P_{02}\eta_y^2\right)^2 \quad (10)$$

Table 5. Equivalent properties.

Case	Equivalent modulus (GPa)	Equivalent density (10^3 kg/m^3)
1	70.52	4.4000
2	105.86	5.6000
3	117.63	6.1299
4	129.95	6.5000
5	140.15	6.7692
6	148.02	6.9714
7	154.03	7.1273
8	158.74	7.2500
9	162.57	7.3484
10	184.66	7.3571

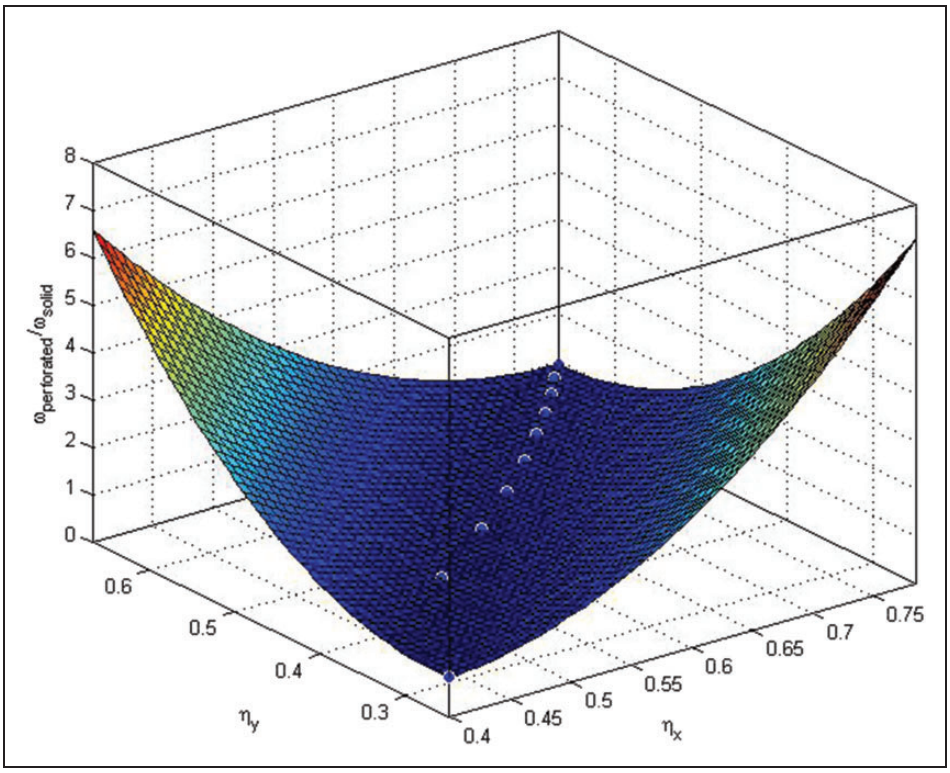

Figure 3. Regression analysis.

Table 6. Equivalent resonant frequencies for the first 20 modes of 10 cases.

	Frequency (rad/s)									
Mode	Case 1	Case 2	Case 3	Case 4	Case 5	Case 6	Case 7	Case 8	Case 9	Case 10
1	1621.9	1761.7	1775.0	1811.7	1843.7	1867.1	1883.7	1896.0	1905.9	2028.6
2	2504.5	2720.3	2740.8	2797.5	2847.0	2883.0	2908.6	2927.7	2942.9	3132.4
3	3971.1	4313.3	4345.8	4435.8	4514.1	4571.3	4611.9	4642.1	4666.2	4966.7
4	3994.6	4338.8	4371.5	4462.0	4540.8	4598.4	4639.2	4669.6	4693.8	4996.1
5	4792.5	5205.5	5244.7	5353.3	5447.8	5516.8	5565.8	5602.3	5631.4	5994.0
6	6053.3	6575.0	6624.5	6761.7	6881.1	6968.2	7030.1	7076.1	7112.9	7570.9
7	6192.6	6726.3	6777.0	6917.3	7039.5	7128.6	7191.9	7239.0	7276.6	7745.2
8	7523.0	8171.4	8233.0	8403.4	8551.8	8660.1	8737.0	8794.2	8839.9	9409.2
9	8171.2	8875.4	8942.3	9127.4	9288.6	9406.3	9489.8	9552.0	9601.6	10220.0
10	8324.0	9041.4	9109.5	9298.1	9462.3	9582.1	9667.2	9730.5	9781.1	10411.0
11	8658.3	9404.6	9475.4	9671.6	9842.4	9967.1	10056.0	10121.0	10174.0	10829.0
12	9680.2	10514.0	10594.0	10813.0	11004.0	11143.0	11242.0	11316.0	11375.0	12107.0
13	10715.0	11638.0	11726.0	11969.0	12180.0	12335.0	12444.0	12526.0	12591.0	13401.0
14	11600.0	12600.0	12695.0	12958.0	13187.0	13354.0	13472.0	13560.0	13631.0	14509.0
15	11801.0	12819.0	12915.0	13183.0	13415.0	13585.0	13706.0	13796.0	13867.0	14760.0
16	12260.0	13316.0	13417.0	13694.0	13936.0	14113.0	14238.0	14331.0	14406.0	15333.0
17	13053.0	14178.0	14285.0	14580.0	14838.0	15026.0	15159.0	15259.0	15338.0	16326.0
18	13812.0	15002.0	15115.0	15428.0	15700.0	15899.0	16041.0	16146.0	16229.0	17274.0
19	14087.0	15301.0	15417.0	15736.0	16014.0	16217.0	16361.0	16468.0	16553.0	17619.0
20	14389.0	15629.0	15747.0	16073.0	16357.0	16564.0	16711.0	16821.0	16908.0	17997.0

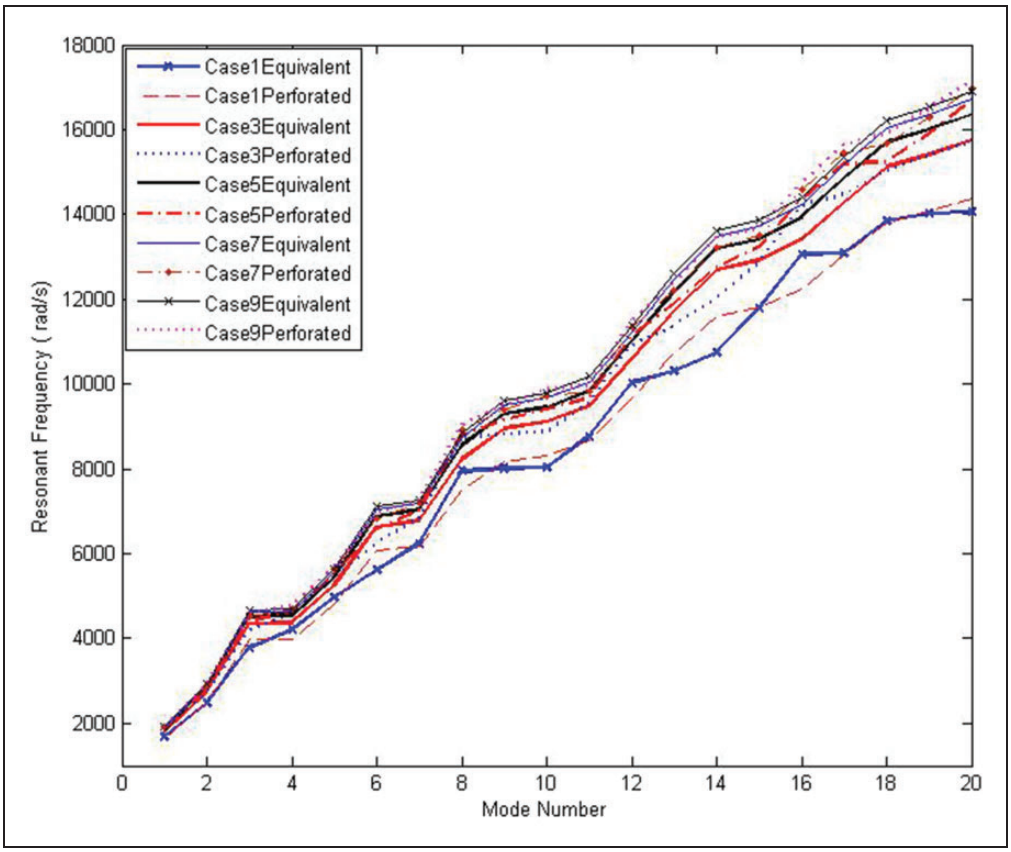

Figure 4. Equivalent versus perforated.

with $P_0 = 1.243$, $P_{10} = -9.769$, $P_{01} = 10.4$, $P_{11} = -75.29$, $P_{20} = 38.23$, and $P_{02} = 36.67$. The equivalent modulus of elasticity (E^*) and the equivalent density (ρ^*) are given in Table 5. Using these equivalent properties in combination with the solid-plate model, the approximated natural frequencies are obtained for each perforation case. The results for all the cases are presented in Table 6. Comparing these results with the exact natural frequencies of the perforated plated yields a maximum average percentage error of 1.3%.

Figure 4 further illustrates the comparison between the equivalent and exact resonant frequencies of perforated plates. Five cases are selected and the results show that the case with the most perforations yields the highest percentage error with a maximum error of 7%. This is an indication that the regression analysis employed to determine the effective elastic modulus is accurate for predicting the equivalent resonant frequencies of perforated plates with rectangular slots and rectangular slot-patterns. The results are applicable for ligament efficiencies varying from 0.25 to 0.8.

Conclusions

Free vibration of perforated plates has been studied by numerous authors. However, most studies are based on circular slots and triangular or square slot-patterns. There is no work on rectangular slots with rectangular slot-patterns. In this paper, the free vibration of perforated plates with rectangular slots and rectangular patterns is examined using finite-element and theoretical analysis. The finite-element analysis is conducted using SolidWorks® Simulations; the natural frequencies are obtained for the solid plate first and then the results are compared with the resonant frequencies obtained theoretically. The results are found to be in excellent agreement, with a maximum percentage error of 0.63%. Ten cases of perforated plates are then modeled in SolidWorks® Simulations to obtain the natural frequencies. As expected, the natural frequencies are smallest for the case with the most perforations.

The natural frequency results of the 10 perforated cases are employed in regression analysis to obtain an explicit expression for the equivalent modulus of elasticity of the perforated plate. These effective elastic constants are then used in solid plates to predict the equivalent resonant frequencies of the 10 perforated cases. The resonant frequencies obtained using the equivalent material properties are found to be in very good agreement with those of the exact resonant frequencies of the perforated plates. This is an indication that the approach employed to predict the equivalent modulus of elasticity is accurate for the study of vibrations of perforated plates.

Declaration of Conflicting Interests

The author(s) declared no potential conflicts of interest with respect to the research, authorship, and/or publication of this article.

Funding

The author(s) disclosed receipt of the following financial support for the research, authorship, and/or publication of this article: The authors would like to acknowledge the financial support of the School of Engineering and Technology at Central Michigan University for supporting the computing facilities to conduct this research.

References

1. O'Donnell WJ and Langer BF. Design of perforated plates. *J Eng Ind* 1962; 84: 307–318.
2. Slot T and O'Donnell WJ. Effective elastic constants for thick perforated plates with square and triangular penetration patterns. *J Manuf Sci Eng* 1971; 93(4): 935–942.
3. O'Donnell WJ. Effective elastic constants for the bending of thin perforated plates with triangular and square penetration patterns. *J Manuf Sci Eng* 1973; 95: 121–128.
4. O'Donnell WJ. A study of perforated plates with square penetration patterns. *Weld Res Counc Bull* 1967; 124: 1089–1101.
5. O'Donnell WJ. Further theoretical treatment of perforated plates with square penetration patterns. *Weld Res Counc Bull* 1970; 151: 1089–1101.
6. Jhung MJ and Yu SO. Study on modal characteristics of perforated shell using effective Young's modulus. *Nucl Eng Des* 2011; 241: 2026–2033.
7. Burgemeister KA and Hansen CH. Calculating resonance frequencies of perforated panels. *J Sound Vib* 1996; 196: 387–399.
8. Sinha JK, Singh S and Rao AR. Added mass and damping of submerged perforated plates. *J Sound Vib* 2003; 260: 549–564.
9. Jeong KH, Ahn BK and Lee SC. Modal analysis of perforated rectangular plates in contact with water. *Struct Eng Mech* 2001; 12: 189–200.
10. Leissa AW. The free vibrations of rectangular plates. *J Sound Vib* 1973; 31: 257–293.
11. Leissa AW and Qatu MS. *Vibration of Continuous Systems*. New York: McGraw-Hill, 2011.
12. Li WL, Zhang X, et al. An exact series solution for the transverse vibration of rectangular plates with general elastic boundary supports. *J Sound Vib* 2009; 321(12): 254–269.
13. Li WL. Vibration analysis of rectangular plates with general elastic boundary supports. *J Sound Vib* 2004; 273: 619–635.
14. Dickinson SM and Li EKH. On the use of simply supported plate functions in the Rayleigh–Ritz method applied to the vibration of rectangular plates. *J Sound Vib* 1982; 80: 292–297.
15. Dickinson SM and Di Blasio A. On the use of orthogonal polynomials in the Rayleigh–Ritz method for the study of the flexural vibration and buckling of isotropic and orthotropic rectangular plates. *J Sound Vib* 1986; 108: 51–62.

16. Dalaei M and Kerr A. Natural vibration analysis of clamped rectangular orthotropic plates. *J Sound Vib* 1996; 189(3): 399–406.
17. Cupial P. Calculation of the natural frequencies of composite plates by the Rayleigh–Ritz method with orthogonal polynomials. *J Sound Vib* 1997; 201: 385–387.
18. Bhat RB. Natural frequency of rectangular plates using characteristic orthogonal polynomials in Rayleigh–Ritz method. *J Sound Vib* 1985; 102(4): 493–499.

Appendix 1

Notation

a	length of plate
b	width of plate
c	height of perforation
d	width of perforation
D	flexural rigidity of plate
E	modulus of elasticity of solid plate
E^*	modulus of elasticity of perforated plate
P_x	distance between two adjacent slots in the x direction
P_y	distance between two adjacent slots in the y direction
α	length over width ratio
ζ	nondimensional coordinate in the x direction
η_x	ligament efficiency in the x direction
η_y	ligament efficiency in the y direction
λ	nondimensional natural frequency
ν	Poisson ratio of plate
ρ	density of solid plate
ρ^*	density of perforated plate
ω	circular natural frequency